Journal of Advanced Marine Engineering and Technology, Vol. 48, No. 5, pp. 302~309, 2024
J. Advanced Marine Engineering and Technology (JAMET)
https://doi.org/10.5916/jamet.2024.48.5.302

ISSN 2234-7925 (Print)
ISSN 2765-4796 (Online)
Original Paper

Corrosion behavior of Zn, Zn-Mg-Al, and Al-Si alloy coated steel sheet in a simulated marine environment

Yeseul Na[1] · Sanjaya Kumar Pradhan[2] · Je-shin Park† · Min-Suk Oh††

(Received September 9, 2024 ; Revised October 10, 2024 ; Accepted October 23, 2024)

Abstract: In this study, we investigated the corrosion behaviors of Zn, Zn-Mg-Al, and Al-Si alloy coatings in a simulated marine environment. Through a combination of electrochemical testing, immersion corrosion experiments, and salt spray tests, it was found that the Zn coatings exhibited inferior corrosion resistance owing to the formation of a porous corrosion layer predominantly composed of ZnO corrosion products, whereas the Al-Si coatings demonstrated superior protective properties, which was attributed to the development of a more effective barrier layer consisting of large, plate-like Al-based oxides. The results showed that the corrosion products formed on each coating significantly influenced the corrosion behavior. Notably, although the corrosion products formed on both Zn-based coating systems, such as the Zn and Zn-Mg-Al coatings, were almost similar, they exhibited markedly different corrosion rates, which can be attributed to variations in the time and quantity of ZnO corrosion product formation. The presence of ZnO appears to inhibit the formation of the dense protective corrosion product, $Zn_5(OH)_6(CO_3)_2$, gradually making the corrosion-product layer more porous. In contrast, the superior corrosion resistance exhibited by the Al-Si coating can be attributed to the formation of large plate-shaped Al-based oxides, which provide a more effective barrier against corrosive environments.

Keywords: Zn, Zn-Mg-Al, Al-Si, Alloy coatings, Corrosion

1. Introduction

Galvanized (GI) steel sheets are widely applied in the marine and shipbuilding industries for various offshore structures that require excellent corrosion resistance **[1]-[4]**. GI steels offer corrosion protection through the sacrificial anode effect, facilitated by the application of a Zn coating **[5]**. Zn, which has a lower electrochemical potential than Fe, is preferentially oxidized, thereby shielding the underlying steel substrate. The resulting Zn oxidation products form a protective layer that acts as a physical barrier, impeding the penetration of corrosive species such as chloride ions into the base metal **[6]-[12]**. This dual mechanism of electrochemical and physical protection makes Zn plating an effective strategy for enhancing the corrosion resistance of steels. Hot-dip galvanized steel sheets are extensively utilized in the automotive industry owing to their cost-effectiveness and ease of production. However, with the increasing severity of industrial environments and consequent demand for materials with superior corrosion resistance, there is a growing demand for research on alternative steel materials that can replace conventional hot-dip galvanizing processes **[13]**.

In response to the demand for enhanced corrosion resistance, Zn-Mg-Al (ZMA) ternary alloy coatings have been developed, which involve the addition of Al and Mg to conventional Zn coatings, resulting in a microstructure comprising a primary Zn phase and a Zn/Al/$MgZn_2$ ternary phase **[12]-[14]**. A ZMA ternary alloy coating was developed to overcome the limitations associated with traditional Zn-coated steel sheets, providing superior corrosion resistance and improved mechanical properties **[15]**. Based on these enhanced characteristics, ZMA ternary alloy coating is extensively utilized across various industrial sectors, demonstrating particularly outstanding performance in environments where corrosion protection is of paramount importance **[12][14]-[19]**.

†† Corresponding Author (ORCID: http://orcid.org/0000-0002-7274-2519): Professor, Division of Advanced Materials Engineering, Department of Energy Storage/Conversion Engineering of Graduate School, Jeonbuk National University, 567, Baekje-daero, Deokjin-gu, Jeonju-si, Jeollabuk-do 54896, Korea, E-mail: misoh@jbnu.ac.kr, Tel: +82-63-270-2297

† Co-Corresponding Author: Professor, Division of Advanced Materials Engineering, Jeonbuk National University, 567, Baekje-daero, Deokjin-gu, Jeonju-si, Jeollabuk-do 54896, Korea, E-mail: parkjs@jbnu.ac.kr, Tel: +82-63-270-2293

1 M. S. Candidate, Division of Advanced Materials Engineering, Jeonbuk National University, E-mail: yeseul0823@jbnu.ac.kr

2 Ph. D. Candidate, Graduate School of Integrated Energy-AI, Jeonbuk National University, E-mail: sanjayap@jbnu.ac.kr

This is an Open Access article distributed under the terms of the Creative Commons Attribution Non-Commercial License (http://creativecommons.org/licenses/by-nc/3.0), which permits unrestricted non-commercial use, distribution, and reproduction in any medium, provided the original work is properly cited.

Copyright ⓒ The Korean Society of Marine Engineering

ZMA ternary alloy coatings exhibit excellent surface corrosion resistance and robust protection at cut edges **[13]**.

In addition to Zn-based alloy coatings, Al-Si alloy coatings, which are produced by adding Si to an Al coating bath, have been developed as a promising alternative for achieving superior corrosion and heat resistance. During the hot-dip aluminizing process, the steel undergoes immersion in a high-temperature Al bath, which induces Fe-Al diffusion and the formation of a thick, irregular intermetallic layer, predominantly composed of Fe_2Al_5 **[20]**. This intermetallic layer is the primary factor contributing to corrosion and mechanical damage. To address these challenges, the addition of Si is employed to decelerate the Fe-Al diffusion rate, thereby inhibiting the growth of the Fe_2Al_5 phase **[21][22]**. In corrosive environments, the Al-Si alloy coatings develop a stable passive film consisting of Al-based oxides or hydroxides, such as Al_2O_3, owing to the preferential oxidation of Al over Fe. This passive layer provides an effective barrier that significantly enhances the corrosion resistance of the coating **[22]-[24]**. Although previous investigations have predominantly focused on salt spray tests (SST) and outdoor exposure studies, these methodologies typically allow for the gradual accumulation of corrosion products that can form a protective physical barrier. However, such accumulation may not accurately represent the dynamic conditions encountered in fluid environments such as seawater. Recognizing this potential discrepancy, our study aims to bridge this gap by conducting immersion tests to evaluate the protective efficacy of corrosion products under conditions that more closely simulate the marine environment. This approach provides novel insights into the corrosion behavior of materials in a simulated marine environment under stirred conditions, where continuous flow may impede the formation of stable protective layers. By examining the corrosion mechanisms and product formation under these conditions, our research offers a more comprehensive understanding of material performance in real-world marine applications, thereby addressing a critical aspect that is often overlooked in traditional corrosion testing methodologies.

In this study, the corrosion behaviors of Zn, ZMA alloy, and Al-Si coatings were examined through immersion tests. The surface microstructures of the corroded samples were subsequently analyzed to identify the corrosion products formed on each type of coated steel sheet. Furthermore, the corrosion resistance of each coated steel sheet was assessed using SST and electrochemical analysis. These methods provide a comprehensive evaluation of the protective performances of different coatings under corrosive conditions.

2. Experimental Method

The chemical compositions of the Zn, ZMA alloy, and Al-Si coatings used in this investigation are listed in **Table 1**. To ensure a standardized evaluation of corrosion resistance, all steel sheets were coated with a uniform coating layer thickness of 7 μm. The coated steel sheets were cut into 25 mm × 25 mm specimens for the corrosion tests. Prior to testing, the specimens were ultrasonicated in acetone and ethanol for 10 min each to eliminate surface contaminants and residual antirust oil. The cross sections and one side of each specimen were treated with an anti-rust primer (KSM-6030) to exclude corrosion caused by the cut edges and to compare only the corrosion behavior of the coated surface.

Table 1: Chemical composition (wt. %) of coatings.

Coatings	Coating thickness	Composition (wt.%)			
		Zn	Mg	Al	Si
Zn	7 μm	99.8	-	0.2	-
ZMA		97	1.5	1.5	-
Al-Si		-	-	91	9

Corrosion tests were conducted in 5 wt. % NaCl solution at 60 °C under stirred conditions. A post-corrosion surface analysis was performed using an optical microscope (Leica DM750, Korea). The phases and microstructures of the corrosion products were characterized using a field-emission scanning electron microscope (FE-SEM, Hitachi SU6600, Japan) equipped with an energy-dispersive spectrometer (EDS). X-ray diffraction (XRD, Rigaku RINT-2000, Japan) with monochromatic Cu-Kα radiation (λ = 0.15406 nm) was employed to analyze the phase composition of the coating surface before and after corrosion.

Electrochemical measurements were performed using a potentiostat (Gamry Interface 1010E, USA) with a three-electrode system consisting of a saturated calomel electrode (SCE) as the reference electrode, graphite as the counter electrode, and the sample as the working electrode. Each specimen was immersed in 3.5 wt. % NaCl solution for 1 h to achieve a stable open circuit potential (OCP) prior to electrochemical impedance spectroscopy (EIS) measurements. EIS) measurements were performed at an OCP of 10 mV with an AC amplitude ranging from 100 kHz to 10 mHz. Potentiodynamic polarization experiments were performed at a sweep rate of 0.3333 mV/s from -0.25 V to 0.3 V (vs.

OCP). The corrosion current density (i_{corr}) and corrosion potential (E_{corr}) were determined using Tafel extrapolation. EIS data analysis and Nyquist plot curve fitting were performed using the Gamry Echem Analyst software (version 7.10.0).

Salt spray testing (SST) was conducted using a salt spray tester (SST, STP-90C-3, Suga) in accordance with ASTM B117 standards. The test was performed at 35 °C using a 5 wt.% NaCl solution with a spray rate of 1.5 ± 0.5 ml/h. Prior to SST, the specimen edges were insulated with tape, leaving an exposed area of 20 mm x 20 mm.

3. Results and Discussion

Figure 1 shows optical micrographs illustrating the progression of corrosion on the zinc-coated, ZMA-alloy-coated, and Al-Si alloy-coated steel specimens as a function of exposure time. The Zn-coated specimens exhibited white corrosion products after 24 h of exposure (**Figure 1b**). However, prolonged exposure for 72 h resulted in the dissolution of these products and the subsequent formation of red rust (**Figure 1c**), indicating substrate corrosion. In contrast, both the ZMA- and Al-Si coated specimens maintained a surface layer of white corrosion products throughout the 72 h exposure period (**Figures 1f** and **1i**, respectively). A notable observation was made at the 24 h mark, where the Al-Si coated specimen (**Figure 1h**) displayed larger corrosion product formations compared to the ZMA specimen (**Figure 1e**). This variation in both coatings suggests the formation of distinct corrosion products on these surfaces, likely owing to differences in the composition and microstructure of the respective coatings.

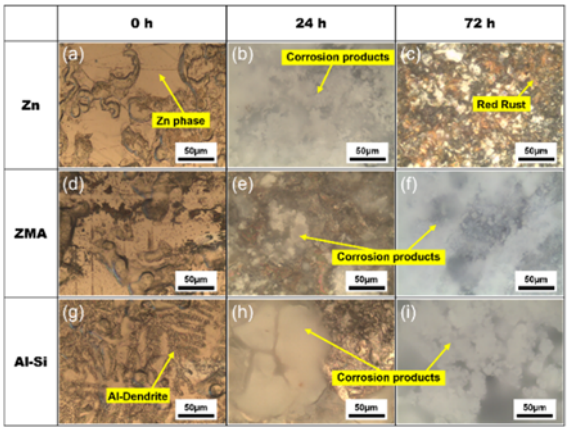

Figure 1: Optical micrographs after corrosion test of Zn, ZMA, Al-Si steels from ((a) - (c)) Zn, ((d) - (f)) ZMA, ((g) - (i)) Al-Si

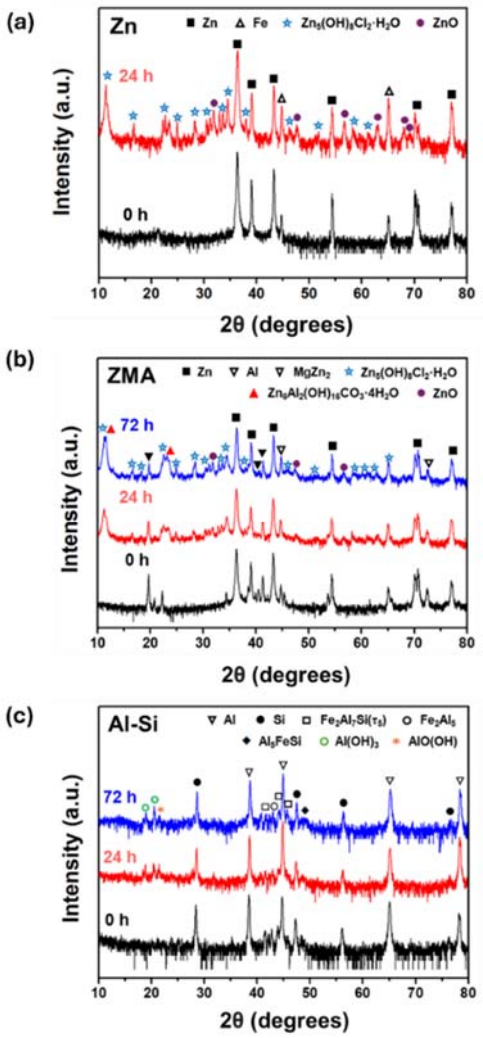

Figure 2: XRD analysis results before (0 h) and after (24 h, 72 h) corrosion test of Zn, ZMA, Al-Si coatings.

Figure 2 shows the XRD analysis results of the specimen surfaces before and after the corrosion test. The XRD data of the Zn coating after 72 h of immersion were omitted because of the visual observation of red rust formation. The unexposed Zn coating exhibited characteristic Zn and Fe peaks, confirming its nature as a typical hot-dip galvanized steel. However, 24 h immersed Zn coating revealed the formation of corrosion products, primarily $Zn_5(OH)_8Cl_2{\cdot}H_2O$ and ZnO. Notably, the number of ZnO peaks observed in the Zn coating was higher than those in the ZMA and Al-Si coatings after 24 h of immersion, suggesting accelerated corrosion in the former. The unexposed ZMA coating predominantly displayed Zn peaks, similar to the Zn coating (0 h), with additional Al and $MgZn_2$ peaks attributed to the Mg and Al alloying elements. However, $Zn_5(OH)_8Cl_2{\cdot}H_2O$ and ZnO were detected for the ZMA coatings immersed for 24 and 72 h peaks immersed ZMA respectively, analogous to the Zn coating (24 h).

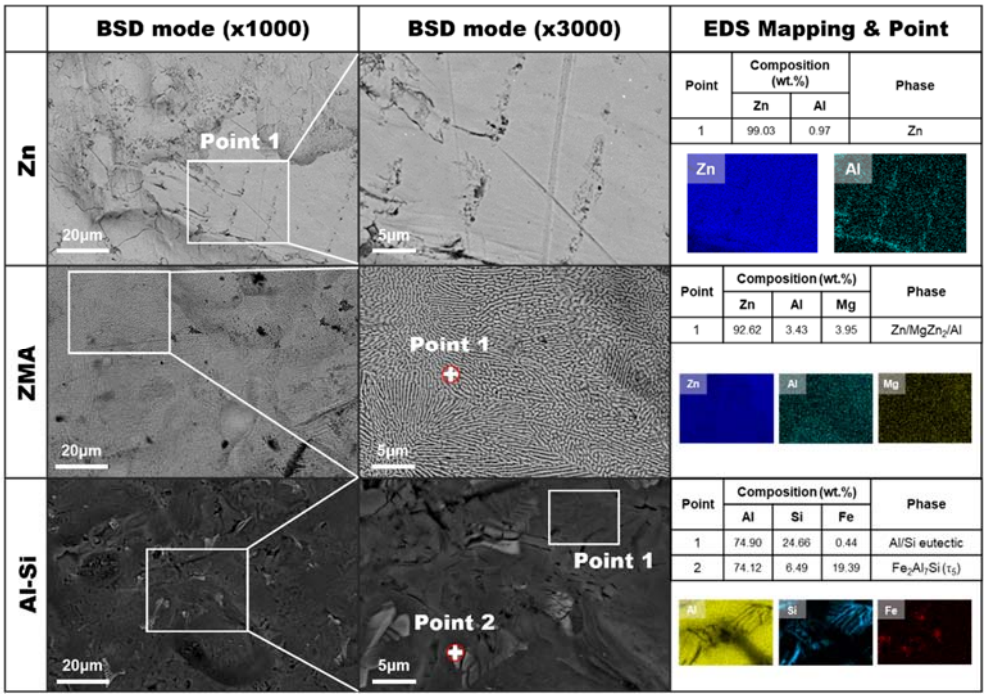

Figure 3: Surficial SEM micrographs of unexposed Zn, ZMA, and Al-Si coatings.

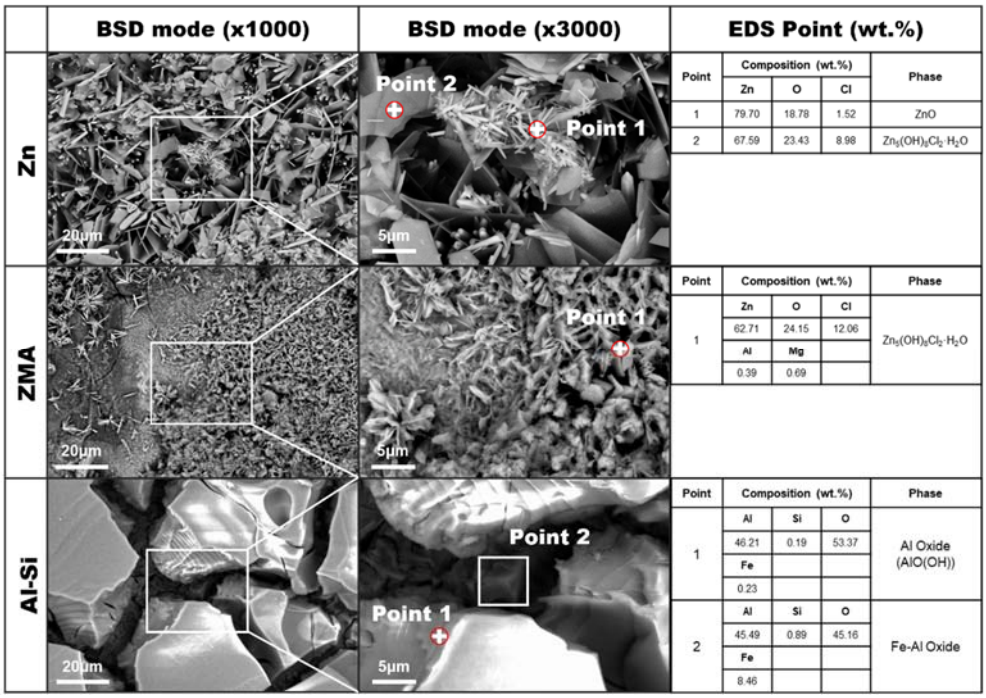

Figure 4: Surficial SEM micrographs of the Zn, ZMA, and Al-Si coatings after exposure to corrosion environment for 24 h.

In particular, the post-corroded ZMA coating uniquely exhibited the $Zn_6Al_2(OH)_{16}CO_3 \cdot 4H_2O$ phase, likely due to the Al addition. The Al-Si coating showed peaks corresponding to the Al, Si, Fe_2Al_7Si, Fe_2Al_5, and Al_5FeSi phases when not exposed to a corrosive environment. However, following the corrosion exposure, the formation of $Al(OH)_3$ and AlO(OH) corrosion products was observed. It is hypothesized that these aluminum hydroxides form a stable passive layer that provides enhanced protection to the underlying coating.

Surface SEM micrographs of the unexposed Zn, ZMA, and Al-Si coatings are shown in **Figure 3**. The EDS maps of the Zn coating revealed predominantly single-phase Zn with trace

amounts of Al. The ZMA coating exhibited the characteristic microstructure of the ZMA alloy coating and a lamellar-shaped Zn/Al/$MgZn_2$ ternary eutectic structure. In contrast, the Al-Si coating displayed a distinct microstructure, with Al serving as the base component. Si particles were segregated at the interface between the Al dendritic structure and the matrix, as confirmed by EDS mapping. Additionally, the Fe_2Al_7Si phase detected by XRD analysis was observed in the Al-Si matrices.

Figure 4 shows surface SEM micrographs of the Zn, ZMA, and Al-Si coatings after exposure to the corrosion environment for 24 h. The formation of rod-shaped ZnO corrosion products seems to deteriorate the corrosion resistance of the Zn coatings owing to their porous nature **[19]**. In contrast, the ZMA coating showed no evidence of ZnO formation. Instead, Simonkolleite ($Zn_5(OH)_8Cl_2{\cdot}H_2O$) was observed; a corrosion product known for its dense structure and superior corrosion resistance properties compared to ZnO **[18]**. The Al-Si coating exhibited corrosion products with larger dimensions than those observed on the ZMA coating, characterized by a plate-like morphology. EDS point analysis identified the corrosion product as (Al(OH)). This Al-based hydroxide is hypothesized to function as a protective barrier, physically impeding contact between Cl^- ions and the underlying material, thereby enhancing corrosion resistance.

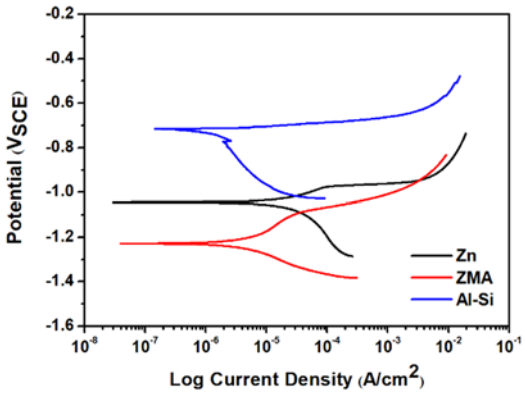

Figure 5: Potentiodynamic polarization plots of unexposed Zn, ZMA, Al-Si coatings.

Figure 5 shows the potentiodynamic polarization plots of the unexposed Zn, ZMA, and Al-Si coatings. **Table 2** presents the calculated E_{corr} and i_{corr} values for the three coating types. i_{corr} is inversely proportional to the corrosion resistance, with lower i_{corr} values indicating superior corrosion resistance. Based on this principle, the corrosion resistance of the coatings can be ranked in descending order as Al-Si > ZMA > Zn. Notably, the Al-Si coating exhibits a lower i_{corr} value than the ZMA coating, suggesting that the corrosion products formed on the Al-Si surface constitute a more stable protective layer. This observation is consistent with the hypothesis that the Al-based corrosion products on the Al-Si sample form a more effective barrier against further corrosion than those formed on the ZMA coating.

Table 2: Electrochemical corrosion parameters of Zn, ZMA, Al-Si coatings.

Sample	E_{corr} (V)	i_{corr} (μA/cm^2)
Zn	-1.040	5.20
ZMA	-1.230	1.43
Al-Si	-0.715	0.873

Figure 6 shows the Nyquist plots of the unexposed Zn, ZMA, and Al-Si coatings. EIS data fitting was performed, and the equivalent circuit model is shown in the inset of **Figure 6**. The electrochemical parameters obtained from the fitted EIS results are listed in **Table 3**. The polarization resistance (R_p) values for Zn, ZMA, and Al-Si coatings were obtained as 1377 Ωcm^2, 3612 Ωcm^2 and 4365 Ωcm^2, respectively. These results indicate that the corrosion resistance follows the order–of Si > ZMA > Zn, which is in good agreement with the previously observed i_{corr} values from the potentiodynamic polarization tests, further indicating the superior corrosion resistance of the Al-Si coating because of its higher value, which suggests a more effective barrier against corrosive processes.

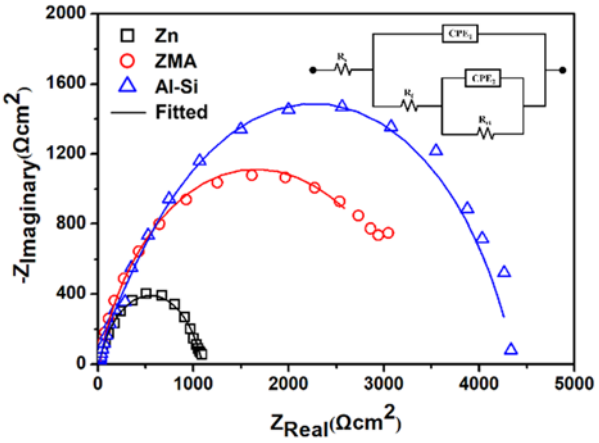

Figure 6: Nyquist plots and equivalent circuit used to fit EIS results of unexposed Zn, ZMA, Al-Si coatings.

The results of the SST conducted to further evaluate the corrosion resistance are shown in **Figure 7**. The Zn coating exhibited the formation of white corrosion products on its surface after

Table 3: Electrochemical parameters estimated from the fitted EIS results (**Figure 6**) of the Zn, ZMA, Al-Si coatings.

Sample	R_s (Ωcm^2)	CPE_f ($\Omega^{-1}cm^{-2}$ S^n)	n_f	R_f (Ωcm^2)	CPE_{dl} ($\Omega^{-1}cm^{-2}$ S^n)	n_{dl}	R_{ct} (Ωcm^2)	R_p (Ωcm^2)
Z	14.57	2.49×10^{-5}	0.81	1,062	5.06×10^{-5}	0.32	315	1,377
ZMA	16.53	8.06×10^{-5}	0.87	1.76×10^{-2}	9.01×10^{-5}	0.49	3,612	3,612
Al-Si	13.25	8.42×10^{-6}	0.85	921	1.75×10^{-5}	0.73	3,444	4,365

only one day of exposure. In contrast, both the ZMA and Al-Si coatings demonstrated remarkable stability, showing negligible visual changes even after seven days of continuous testing. This pronounced difference in corrosion-product formation and surface stability provides compelling evidence for the superior corrosion resistance of the ZMA and Al-Si coatings compared with that of the conventional Zn coating. The extended period of surface integrity maintained by the ZMA and Al-Si coatings under aggressive salt spray conditions validated the electrochemical test results, further confirming their enhanced protective capabilities in corrosive environments.

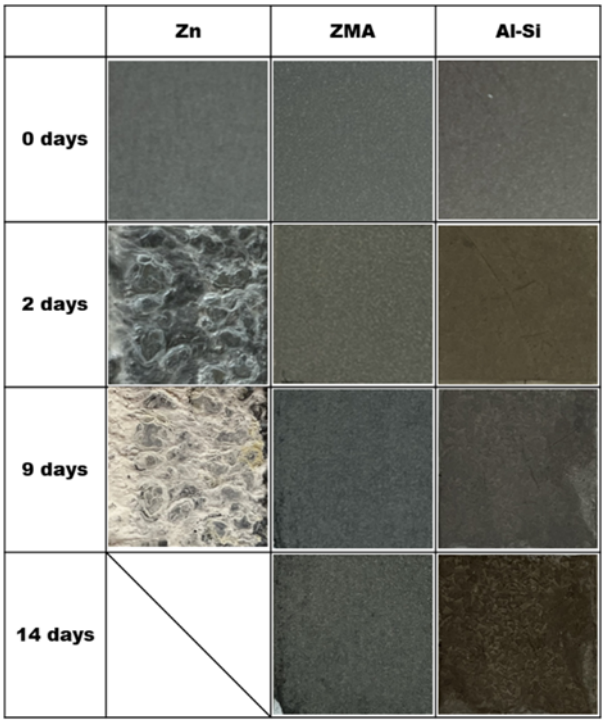

Figure 7: SST results of the Zn, ZMA, Al-Si coatings

The corrosion behaviors of the Zn, ZMA, and Al-Si alloy coatings were investigated through surface microstructural analysis and corrosion product characterization. It can be concluded that the distinct corrosion product formation mechanisms observed in each coating system provide insights into their respective corrosion resistance properties, with the more stable and less porous corrosion products of the ZMA and Al-Si coatings conferring superior protection against corrosive environments.

4. Conclusion

This study investigated the corrosion behavior of Zn, ZMA, and Al-Si alloy coatings in a simulated marine environment through surface microstructural analysis and corrosion product characterization. The immersion corrosion test, SST, and electrochemical analyses consistently demonstrated the superior corrosion resistance of the ZMA and Al-Si coatings compared with the conventional Zn coating. This difference in corrosion resistance can be attributed to the distinct nature of the corrosion products formed during the corrosion process.

The XRD phase analysis revealed a higher prevalence of the ZnO phase in the Zn coating than in the ZMA coating. SEM observations indicated that the ZnO corrosion products exhibited a more porous morphology than the $Zn_5(OH)_8Cl_2 \cdot H_2O$ formed on the ZMA coating. This porous structure of ZnO likely contributes to the decreased corrosion resistance of the Zn coating.

In the case of the Al-Si coating, XRD and SEM-EDS analyses identified the formation of $Al(OH)_3$ and AlO(OH) as corrosion progressed. These aluminum hydroxides appeared to form a protective barrier layer, enhancing the overall corrosion resistance of the Al-Si coating.

Acknowledgement

This work was supported by National Research Foundation (Korea), funded by Ministry of Science and ICT (2022R1A2C1008972) and supported in part by Technology Development Program (00221849) funded by Ministry of SMEs and Start-ups (MSS, Korea).

Author Contributions

Conceptualization, Y. S. Na; Methodology, S. K. Pradhan; Formal Analysis, Y. S. Na; Investigation, S. K. Pradhan; Data

Curation, M. S. Oh; Writing-Original Draft Preparation, Y. S. Na and S. K. Pradhan; Writing-Review & Editing, M. S. Oh; Supervision, J. S. Park; Funding Acquisition, M. S. Oh.

References

[1] Y. Liu, A. Ooi, E. Tada, and A. Nishikata, "Electrochemical monitoring of the degradation of galvanized steel in simulated marine atmosphere," Corrosion Science, vol. 147, pp. 273-282, 2019.

[2] I. O. Wallinder and C. Leygraf, "A critical review on corrosion and runoff from zinc and zinc-based alloys in atmospheric environments," Corrosion, vol. 73, no. 9, pp. 1060-1077, 2017.

[3] L. Maldonado, M. A. Pech-Canul, and S. Alhassan, "Corrosion of zinc-coated reinforcing bars in tropical humid marine environments," Anti-Corrosion Methods and Materials, vol. 53, no. 6, pp. 357-361, 2006.

[4] A. Diaconu, C. Solomon, L. Benea, V. DUMITRAŞCU, and L. MARDARE, "Corrosion resistance of zinc coated steel in sea water environment," The Annals of "Dunarea de Jos" University of Galati, Fascicle IX, Metallurgy and Materials Science, vol. 38, no. 3, pp. 34-39, 2015.

[5] Y. Liang, B. He, G. Fu, S. Wu, B. Fan,"Effects of ambient temperature and state of galvanized layer on corrosion of galvanized steel in high-humidity neutral atmosphere," Materials, vol. 16, no. 10, 3656, 2023.

[6] D. Persson, D. Thierry, and O. Karlsson, "Corrosion and corrosion products of hot dipped galvanized steel during long term atmospheric exposure at different sites worldwide," Corrosion Science, vol. 126, pp. 152-165, 2017.

[7] D. De la Fuente, J. G. Castano, and M. Morcillo, "Long-term atmospheric corrosion of zinc," Corrosion Science, vol. 49, no. 3, pp. 1420-1436, 2007.

[8] S. Tailor, A. Modi, and S. C. Modi, "Synthesis, microstructural, corrosion and antimicrobial properties of Zn and Zn–Al coatings," Surface Engineering, vol. 35, no. 8, pp. 736-742, 2019.

[9] K. Zhang, R. Song, and Y. Gao, "Corrosion behavior of hot-dip galvanized advanced high strength steel sheet in a simulated marine atmospheric environment," International Journal of Electrochemical Science, vol. 14, no. 2, pp. 1488-1499, 2019.

[10] N. C. Hosking, M. A. Ström, P. H. Shipway, and C. D. Rudd, "Corrosion resistance of zinc–magnesium coated steel," Corrosion Science, vol. 49, no. 9, pp. 3669-3695, 2007.

[11] W. Ni, P. Li, Y. Zhu, Z. Di, L. Guo, and Y. Liu, "Comparative study of anti-corrosion properties and lifespan prediction model for inorganic zinc-rich coating and thermal-spray zinc coating," Coatings, vol. 12, no. 4, 505, 2022.

[12] Y. Meng, L. Liu, D. Zhang, C. Dong, Y. Yan, A. A. Volinsky, and L. N. Wang, "Initial formation of corrosion products on pure zinc in saline solution," Bioactive Materials, vol. 4, pp. 87-96, 2019.

[13] S. Schürz, M. Fleischanderl, G. H. Luckeneder, K. Preis, T. Haunschmied, G. Mori, and A. C. Kneissl, "Corrosion behaviour of Zn–Al–Mg coated steel sheet in sodium chloride-containing environment," Corrosion Science, vol. 51, no. 10, pp. 2355-2363, 2009.

[14] C. Yao, H. Lv, T. Zhu, W. Zheng, X. Yuan, and W. Gao, "Effect of Mg content on microstructure and corrosion behavior of hot dipped Zn–Al–Mg coatings," Journal of Alloys and Compounds, vol. 670, pp. 239-248, 2016.

[15] T. Guo, Y. Wang, L. Yu, Y. Jin, B. Zeng, B. Dou, X. Liu, X. Lin, "Roles of Al and Mg on the microstructure and corrosion resistance of Zn-Al-Mg hot-dipped coated steel," Materials, vol. 17, no. 7, 1512, 2024.

[16] S. Wang, X. Ma, J. Bai, T. Du, R. Ma, A. Du, and G. Li, "Study of the corrosion behavior and mechanism of a hot-dipping Zn–6Al–3Mg alloy coating in 3.5 wt% neutral NaCl solution," Surface and Coatings Technology, vol. 464, 129576, 2023.

[17] M. Uranaka, and T. Shimizu, "Corrosion resistance of hot-dip Zn-6% Al-3% Mg alloy coated steel sheet used in automotive parts," Metallurgical Science and Technology, vol. 30, no. 1, 2012.

[18] N. LeBozec, D. Thierry, D. Persson, C. K. Riener, and G. Luckeneder, "Influence of microstructure of zinc-aluminium-magnesium alloy coated steel on the corrosion behavior in outdoor marine atmosphere," Surface and Coatings Technology, vol. 374, pp. 897-909, 2019.

[19] P. Volovitch, C. Allely, and K. Ogle, "Understanding corrosion via corrosion product characterization: I. case study of the role of Mg alloying in Zn–Mg coating on steel," Corrosion Science, vol. 51, no. 6, pp. 1251-1262, 2009.

[20] J. Duchoslav, R. Steinberger, M. Arndt, T. Keppert, G. Luckeneder, K. H. Stellnberger, and D. Stifter, "Evolution of the surface chemistry of hot dip galvanized Zn–Mg–Al

and Zn coatings on steel during short term exposure to sodium chloride containing environments," Corrosion Science, vol. 91, pp. 311-320, 2015.

[21] W. J. Cheng and C. J. Wang, "Growth of intermetallic layer in the aluminide mild steel during hot-dipping," Surface and Coatings Technology, vol. 204, no. 6-7, pp. 824-828, 2009.

[22] W. J. Cheng and C. J. Wang, "Observation of high-temperature phase transformation in the Si-modified aluminide coating on mild steel using EBSD," Materials Characterization, vol. 61, no. 4, pp. 467-473, 2010.

[23] W. J. Cheng and C. J. Wang, "Microstructural evolution of intermetallic layer in hot-dipped aluminide mild steel with silicon addition," Surface and Coatings Technology, vol. 205, no. 19, pp. 4726-4731, 2011.

[24] Y. Tak, J. Kang, and J. Choi, "Electrochemical properties of metal aluminum and its application," Applied Chemistry for Engineering, vol. 17, no. 4, pp. 335-342, 2006.

[25] V. G. Shmorgun, A. I. Bogdanov, A. O. Taube, and R. E. Novikov, "Investigation of heat resistance of Al-Ni layered coating," Solid State Phenomena, vol. 265, pp. 211-214, 2017.